A STUDY OF THE SURFACE MORPHOLOGY OF SILICON: EFFECT OF PARASITIC EMITTER ETCHING ON THE REAR-SIDE PERFORMANCE OF SILICON SOLAR CELLS

A. Dastgheib-Shirazi, M. Steyer, J. Junge, S. Gindner, G. Hahn
University of Konstanz, Department of Physics, Jacob-Burckhardt-Str. 29, 78464 Konstanz, Germany
amir.dastgheib-shirazi@uni-konstanz.de, Tel.: +49 7531 882088, Fax: +49 7531 883895

ABSTRACT: Silicon solar cells with dielectric passivation layers need enhanced rear surface treatment. In this work we will introduce a novel masking and etching procedure whereby the parasitic emitter etching, the increase of the rear reflectance and finally the improvement of the rear surface passivation will be merged in only one step. Using adapted acidic etching solutions we can show a higher etch rate at pyramid peaks of textured rear sides. This selectivity of the etch rate will allow significant change of the surface morphology without increased material loss. This fact makes the application of thin solar cells more attractive. This novel method is transferred not only to screen-printed solar cell concepts with full area Al-BSF, but also to solar cells with dielectrically passivated rear sides.
The rounding effect of the rear side texture with minimized abrasion leads to high rear side reflectance and increased surface passivation of dielectrically passivated solar cells. A significant gain of 0.5 mA/cm² of solar cells with an adapted rear side morphology confirms the mentioned advantages of this novel etching procedure with masking.
Keywords: parasitic emitter etching, surface passivation, internal reflectance, surface morphology

1 INTRODUCTION

There are certain indispensable process steps in solar cell fabrication, such as the removal of parasitic emitter diffusion and the rear side surface treatment of dielectric passivation layers, which are performed in high efficiency silicon solar cell processes. These steps have to be applied for conventional screen-printed solar cells as well to allow higher efficiencies. During the last few years, various processes for wet inline edge isolation have been introduced and transferred to industrial production. In this study, we focus on a new method to eliminate parasitic emitter diffusion on the rear, increase internal reflectance and at the same time improve the rear-surface passivation of silicon solar cells. With this procedure, parasitic emitter diffusion is completely eliminated, and there is a significant change in surface morphology, which causes an improvement in rear surface passivation and an increase in internal reflectance. One of the main advantages of this novel etching method is the combination of minimized abrasion with maximized rear side reflectance which is made possible by the shiny rear side. For this reason, a low material loss of a few microns is also a prerequisite for future thin rear-side passivated silicon solar cells.

In the following work the behavior of different acidic etching solutions on the surface morphology will be studied. Then a novel rear side etching method with front side masking will be introduced and investigated.

It is well known that in case of a textured surface, the recombination rate at the surface strongly increases which plays a big role for rear side passivated solar cells [5,11]. For that reason the influence of the surface morphology on the surface recombination velocity is also investigated. Finally, the effect of different surface morphologies on the passivation quality will be studied on rear side passivated silicon solar cells.

2 ACIDIC ETCHING SOLUTIONS

In the first study, different acidic etching solutions are applied to ensure homogeneous and complete silicon etching. Thereby the etching kinetics and abrasion are monitored. The purpose of this experiment is to study the dependence of the etching rate and the surface morphology on several different etching solutions.

The wafers used in this study were p-type Cz silicon wafers with a random pyramid texture. Their base resistance was about 2.8 Ωcm, and they were 200 µm thick.

The following diagram shows the process sequence of the first experiment, in which the influence of various etching media on etching removal, surface morphology and finally reflectance is investigated**.**

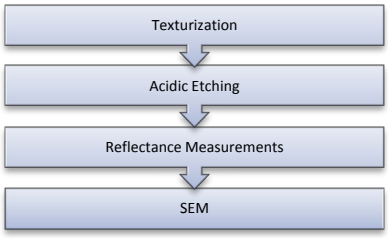

Figure 1: Process sequence of reflectance measurements of symmetrically etched wafers. In addition scanning electron microscopy shows the influence of the etching solution on the surface morphology.

In Figure 1 the process sequence of the first experiment is depicted. After texturization the wafers were symmetrically etched in several different acidic etching solutions.

To ensure homogeneous etching, the procedure was performed at a defined time after the etching solution was mixed.

Next, reflectance measurements and SEM (scanning electron microscope) images were made which will be discussed in detail. The selection of the etching solutions was made according to the following criteria: First, we wanted to minimize material removal, but at the same time achieve a maximal rounding of the random pyramids. In these studies the etching period amounts to less than 250 s.

An examination of SEM images of differently etched pyramids with nearly the same etching removal showed that there is a strong selectivity in etching with regard to pyramid peaks and pyramid valleys.

The main etching solution that we used in these experiments consists of HNO_3 and HF with non-organic additives.

The acidic etching procedure of HNO_3/HF systems can be described by the following reaction:

(a) $3Si + 4HNO_3 \rightarrow 3SiO_2 + 4NO + 2H_2O$
(b) $SiO_2 + 6HF \rightarrow H_2SiF_6 + 2H_2O$

The etching procedure begins with the oxidation of silicon to SiO_2 by HNO_3 (nitric acid). During this reaction (a) nitrogen monoxides and water are the first reaction products, which play an important role for homogenization of the etching solution [16,17,18].

In the second step the SiO_2 is dissoluted by HF. In this reaction (b) H_2SiF_6 (hexafluorosilicic acid) and water are the reaction products. It has to be mentioned that the reaction equations can differ from the above reaction by influence of etching temperature or by additives.

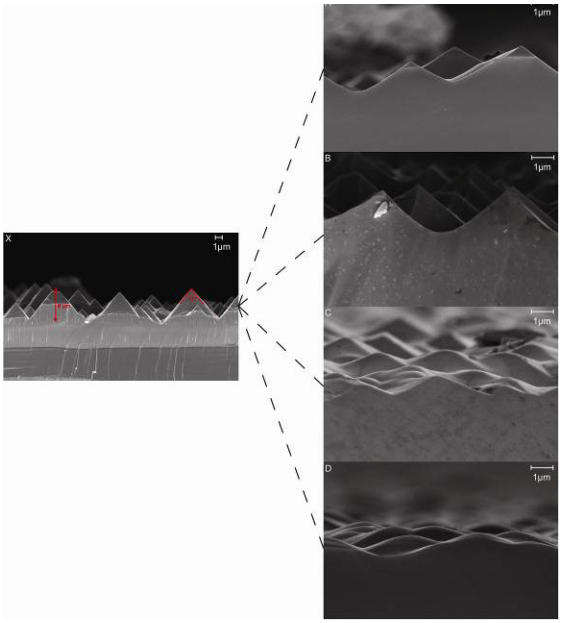

Figure 2: SEM images of various surfaces etched in several different acidic etching solutions. Despite the nearly identical material removal, we detected strong variations in the surface morphology. The acidic etching solutions show variations in the etching rates at the pyramid peaks and in the pyramid valleys.

The left image in Figure 2 shows the original random pyramid texture with a pyramid height of about 7 µm.

Sample A was etched with an increased HF concentration. As we can see, the increase in the HF concentration does not lead to an increased etching rate at the pyramid peaks, but rather to a homogenous etching along the pyramid facets. After an etching time of only 60 s, 9.2 µm of material was already removed from a wafer side. The value of 9.2 µm was calculated from weight measurements before and after the etching procedure. Considering the increase of the surface area in case of a pyramidal textured wafer (factor 1.73), the material loss can only be an upper value for the loss in thickness. We assume that the real abrasion should be much lower. Despite the high removal, after the etching of sample A we can still clearly see the pyramid structure with the sharp-cornered pyramid side surfaces.

Sample B was etched for 240 s in an acidic etching solution diluted with H_2O. Here the pyramid structure is still clearly visible after etching as well. The etching behavior strongly resembles the etching behavior of etching solution A (increased HF concentration), whereby here (solution A) the duration of etching was reduced by a factor of four with the same amount of material removal. In addition, by adding H_2O we can decrease not only the rate of etching, but also reduce the formation of nitric oxide and hydrogen. These gases can accumulate on the pyramid peaks as masking layers, and there can also be selectivity in the etching rate (peak and valley).

Compared with the first two samples, sample C displays a rounded pyramid structure. By the introduction of additives it is possible to increase the etching rate on the pyramid peaks as opposed to the etching rates in the pyramid valleys, whereby with an etching duration of <250 s a clearly visible rounding of the pyramid structure is already achievable.

However, in the same etching period of 250 s the material removal can be reduced by ca. $45\%_{rel}$ by a further adaptation of the etching solution (same etching temperature). With this group D, a clear rounding of the pyramid structure was achieved through an increased etching rate at the pyramid peaks. An adequate rounding of the pyramid structure of the solar cell rear sides for increased rear side reflectance and increased rear side passivation can, however, already be achieved with reduced etching times:
(<120 s and material loss <4 µm).

Table I: Overview of the material loss and the reflectance of the etched samples. A higher etch rate at the pyramid peaks than in the pyramid valleys leads to decreased material loss and higher reflectance. We assume a much lower material loss than the calculated values of material loss from weight measurements before and after the etching procedure.

Etch (time)	Material loss (upper limit) (single side) [µm]	Reflectance @ 1000 nm [%]
X (textured Cz wafer)	-	10
A (60 s)	9.2	29
B (240 s)	9.9	29
C (240 s)	10.3	32
D (240 s)	7.1	32
B (120 s)	5.5	22
C (120 s)	5.4	29
D (120 s)	3.7	27
D (60)	2.2	21

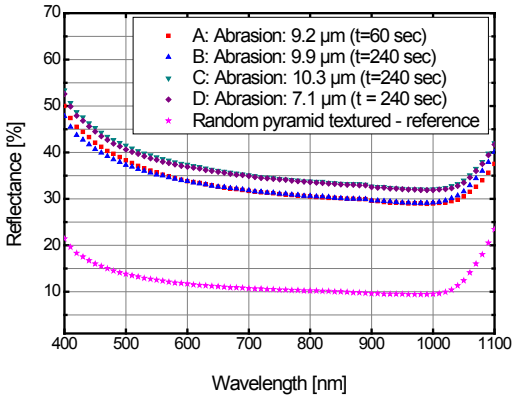

Figure 3: Reflectance measurements of various surfaces etched in several different acidic etching solutions. Comparison of reflectance measurements with Fig. 2 show that samples C & D with rounded pyramids have the highest value of reflectance. However, sample D shows the same high reflectance in the whole wavelength range in spite of a material loss reduction of 45%$_{rel}$.

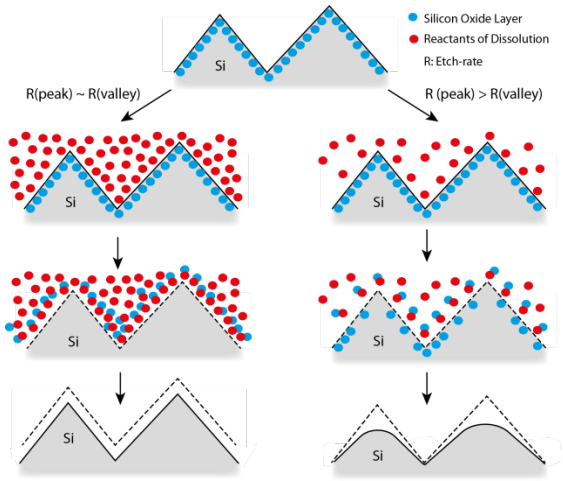

Figure 4: Illustration of two different acidic etching procedures. The left modeling describes a non-optimized acidic etching whereby the etch rate at the pyramid peak is equal to the etch rate in the pyramid valley. In contrast, on the right figure the etch rate at the pyramid peak is much higher than in the pyramid valley. This more optimized acidic etch behavior leads to a significant rounding of the pyramid texture without an increase of the material loss.

Figure 4 shows a modeling of two different acidic etching behaviors. Here we assume that the surface is completely oxidized by HNO_3 (blue points). If the concentration of reactants of dissolution (red points) like HF is increased then pyramid peak, pyramid valley, and the pyramid facets will be etched with the same etch rate. In this case the mass transport intensity is isotropic. The etching solution A in Figure 2 could have a similar etching behavior.

On the other hand the etch rate at the pyramid peaks can be much higher than in the pyramid valleys like shown in the right modeling in Figure 4. In this case the concentration of reactants of dissolution is decreased, whereby the mass transport intensity at the pyramid peaks increases. This could lead to a preferred etching at the pyramid peaks, like the etching solution D in Figure 2.

3 PARASITIC EMITTER ETCHING

The novel rear side emitter etching procedure can be transferred not only to screen-printed solar cell concepts with full area Al-BSF, but also and naturally above all to solar cells with dielectrically passivated rear sides. Furthermore, this procedure can also be combined with the SECT procedure [2,7]. The SECT procedure is a solar cell concept with a selective emitter, whereby the non-masked and thereby non-contacted area of the emitter is wet-chemically etched back on the nanometer scale.

For the novel rear side etching procedure the front side of a solar cell has to be masked, whereby this masking step can be combined with other masking steps during the solar cell processing. Afterwards the rear emitter is etched back in an adapted acidic solution. The advantage of this procedure is the significant change of the surface morphology which has a significant influence on the rear side performance of rear side passivated solar cells.

When applying the procedure, care must be taken that the front side emitter is not damaged during the short etching period. To be sure of this, in the next experiment the sheet resistance is measured before and after the rear side etching.

A critical issue for the emitter etching and the rounding process of the rear side texture is the masking of the front side and its resistance to acidic etching solutions.

For the following experiment we used not only standard $POCl_3$ emitters with R_{sheet}=48 Ω/sq and 80 Ω/sq, but also a higher ohmic etch-back emitter with R_{sheet}=80 Ω/sq, as it is used with the selective emitter concept SECT.

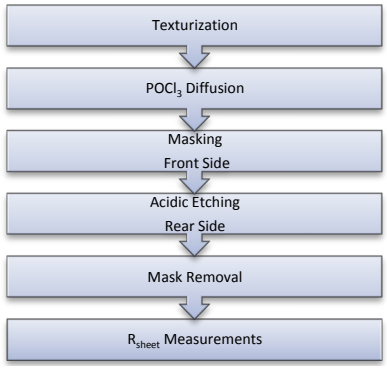

Figure 5: Process sequence of test for front emitter masking.

Table II: R_{sheet} measurements on three different front side $POCl_3$ emitters whose rear side emitters were completely etched back.

$POCl_3$ diffusion	$R_{sheet\text{-}front\ side}$ [Ω/sq] before rear-side etching	$R_{sheet\text{-}front\ side}$ [Ω/sq] after rear-side etching
48 Ω/sq	48.1±0.4	48.3±0.5
80 Ω/sq	80.2±1.2	80.6±1.3
80 Ω/sq Etched Back	80.4±1.4	80.8±1.6

Table II indicates that front side masking offers very satisfactory protection against acidic etching solutions. Sheet resistance measurement was performed on random pyramid textured Cz wafers (R_B=2.8 Ωcm) with a thickness of ca. 200 µm. The very low variation in sheet resistance before and after etching of the rear side and stripping of the mask shows that the etching method with masking can in principle be integrated into solar cell processes.

3.1 Screen-printed solar cell process

In the next step, the novel method is transferred to a screen-printed solar cell process with a full area Al-BSF. Despite the decreased effect of the rear side morphology on the rear side performance of screen-printed solar cells with a full area Al-BSF, the method can be evaluated with regard to one-sided emitter etching.

For this solar cell process we used Cz wafers with random pyramid texture. The base resistivity is about 2.8 Ωcm and the wafers are about 200 µm thick.

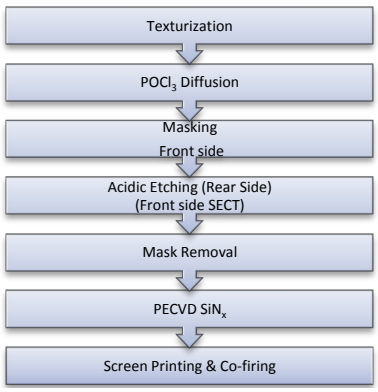

Figure 6: Process sequence of screen-printed solar cells with novel rear side emitter etching. By the selection of suitable etching masks, the procedure can also be combined with the SECT selective emitter concept.

Table III: Mean IV characteristics of large area screen-printed solar cells with homogenous emitter and full area Al-BSF. The novel rear side etching method was transferred to these solar cells.

	V_{oc} [mV]	j_{sc} [mA/cm²]	FF [%]	η [%]	R_{shunt} [mΩcm²]
Mean values	632	37.2	79.1	18.6	$>10^4$

The high values for the shunt resistance ($>10^4$ mΩcm²) of the screen-printed solar cells show that the parasitic emitter junction has been completely removed in the adapted etching solution. The high efficiency of 18.6% of large area screen-printed solar cells (125x125 mm²) shows that the process can be successfully transferred to the industrial screen-printing process with homogenous or selective emitters.

Nevertheless, the full potential of the adapted rear-side structure is reserved for rear side passivated solar cells. The application of this rear side emitter etching to rear side passivated solar cells with local rear contacts would increase their efficiency by increased rear side reflectance and a reduced surface recombination velocity. In the next experiment we study the influence of rear side etching on the effective lifetime and the surface recombination velocity.

4 LIFETIME EXPERIMENT

In the following experiment, the influence of etching on the effective lifetime of symmetrical FZ and Cz samples is investigated. The etching durations are kept within the industrially applicable time frame.

The samples used in this study were p-type FZ wafers, 2.0 Ωcm, {100}, with random pyramid texture and a thickness of 513 µm. The wafers were etched back in an adapted acidic etching solution from the previous studies (Etching solution D) using different etching times. Afterwards, different cleaning procedures were employed, such as IMEC [15] or RCA clean. Finally, the surfaces of the wafers were passivated with the following passivation layers:
PECVD SiN_x (n_{633}=2.25, 70–80 nm), thermal SiO_2 (110 nm), iodine-ethanol, a-Si (30 nm), and Al_2O_3, (30 nm). The iodine-ethanol passivation shows the effect of chemical passivation by the saturation of dangling bonds. Finally, carrier lifetime measurements were performed with QSSPC measurements at a low injection level of $\Delta n = 1 \cdot 10^{15}$ cm^{-3} which is representative of the real injection level of a silicon solar cell. In this case the transient photoconductance method was used [1,3,6,11,12, 13, 14].

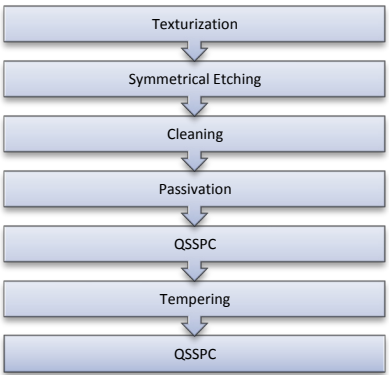

Figure 7: Process sequence of the lifetime experiment.

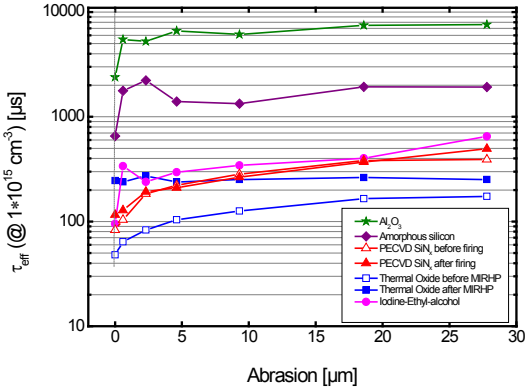

Figure 8: Effective carrier lifetime of symmetrically passivated FZ samples with different surface morphologies.

Figure 8 shows the increase in the effective carrier lifetime of passivated samples with a change in surface morphology. Thereby nearly all samples display similar behavior. The effective carrier lifetime of the samples studied shows a strong increase with an abrasion of less than 5 µm. Consequently, there is a saturation of the effective carrier lifetime. This behavior is very clearly observable for Al_2O_3 passivated surfaces. Only the samples which are passivated by the thermal SiO_2 and annealed by MIRHP do not show the expected increase of τ_{eff} with increased abrasion. Additional investigations on this group have shown that this effect is due to a strong decrease of the effective lifetime of the FZ material after the thermal oxidation which was caused by a non-recurring bulk contamination. In this case (SiO_2 after MIRHP) the very low bulk lifetime of the FZ wafer compensates the surface passivation effect.
An abrasion (single side) of less than 3 µm leads to a significant increase in the effective carrier lifetime to above 5 ms. In order to better evaluate the effects of the surface morphology (rounding of the pyramid structure) on the passivation effect of the samples and above all independently of wafer thickness, the surface recombination velocity was calculated from the τ_{eff} values.

The values for the surface recombination velocity S_{pass} were determined using the following equation [1].

$$S_{pass} = \frac{W}{2} \cdot \left(\frac{1}{\tau_{eff}} - \frac{1}{\tau_{Bulk}} \right)$$

$\tau_{Bulk} >> \tau_{eff}$, τ_{eff} @ $\Delta n = 1 \cdot 10^{15}$ cm^{-3}
W: Wafer thickness

Using FZ wafers we assume no bulk recombination, so the equation can be reduced to:

$$S_{pass} = \frac{W}{2} \cdot \left(\frac{1}{\tau_{eff}} \right)$$

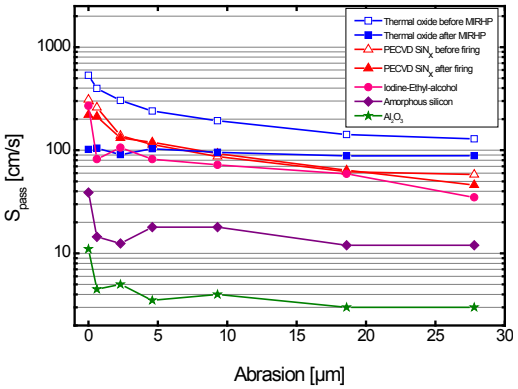

Figure 9: Calculated surface recombination velocities S_{pass} of symmetrically passivated FZ samples with different surface morphologies.

In Figure 9 we can see the dependence of S_{pass} on the material removal and thereby on the surface morphology. It thereby becomes clear that the S_{pass} values are definitely strongly reduced with the marginal removal of just a few µm. If we examine the results more closely, we further see that the first strong reduction of the S_{pass} already occurs after a removal of <1 µm.

The further reduction of the S_{pass} values in Figure 9 can be explained by the change in surface morphology due to the reduction of {111} crystal orientation and the surface area. Furthermore, with the passivation layers that also passivate the base-doped surface via the field effect like SiN_x, SiO_2, and Al_2O_3, the surface morphology can be correlated with the density of surface states D_{it} and the density of fixed surface charges Q_f [13]. This hypothesis must, however, first be verified through CV measurements.

Next, the effective surface recombination velocity S_{eff} for a locally metalized and passivated surface was calculated using the Fischer model [4]. Calculations refer to p-type 2.0 Ωcm FZ and to p-type 2.8 Ωcm Cz silicon. Both materials have a random pyramid texture which is etched back step by step in an adapted etching solution. The calculation includes a contact formation via laser fired contacts after the dielectric passivation and evaporation of aluminum.

$$S_{eff} = \frac{S_{pass}}{1-f} + \frac{D_e}{W} \cdot \left(\frac{l_{rc}}{2W\sqrt{\pi f}} \arctan\left(\frac{2W}{l_{rc}} \sqrt{\frac{\pi}{f}} \right) - e^{\left(-\frac{W}{l_{rc}}\right)} + \frac{D_e}{S_{met} W f} \right)^{-1}$$

$$S_{met} = S_0 + \alpha e^{\beta (N_A + N_0)}$$

S_0 = -900 cm/s
α = 22.1 cm/s
$\beta = 1.29 \cdot 10^{-16}$ cm^{-3}
$N_0 = 3.40 \cdot 10^{16}$ cm^{-3}
N_A: base doping concentration
S_{pass}: surface recombination velocity
f: metallization fraction: 2.5%
D_e: diffusion constant of minority carriers
D_e (2.0 Ωcm): 29.81 cm^2/s
D_e (2.8 Ωcm): 30.96 cm^2/s
W: wafer thickness: 200 µm
l_{rc}: rear contact length: 1 mm

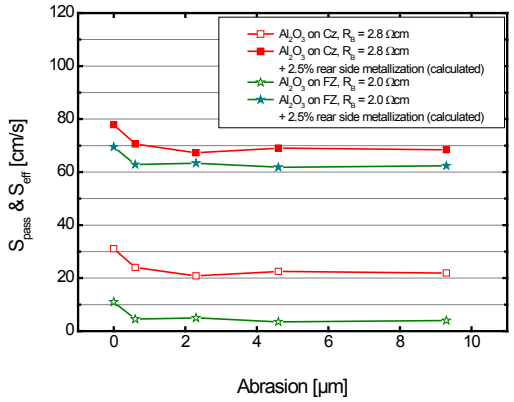

Figure 10: Calculated S_{eff} of Al_2O_3 passivated FZ and Cz material. The calculation parameters are listed above.

Figure 10 illustrates the influence on the surface morphology on S_{pass} and S_{eff} (metalized) of FZ and Cz wafers symmetrically passivated with Al_2O_3. An abrasion of less than 2 µm leads to a significant reduction of S_{eff}.

Based on previous studies, we conclude that the τ_{eff}, S_{pass} and S_{eff} (metalized) are highly dependent on the surface morphology. At the same time, we have shown that for etched surfaces there is a saturation of the decrease in the surface recombination velocity.

5 REAR SIDE PASSIVATED CELLS

The previous experiments have shown that the application of an adjusted etching solution with a minimal material loss (<5 µm on one side) can lead to adequate rounding of the rear side texture. Thereby high reflectance values could be measured on unpassivated and non-metalized samples. Furthermore, we were able to show that by applying adapted etching solutions, the surface recombination velocity could be significantly reduced already after removing of just a few µm.

The aim of the next experiment is to transfer the method of rear side etching with masking to the photolithography-based high efficiency process of the University of Konstanz [8]. Our aim was to test the influence of three different surface morphologies on the internal quantum efficiency (IQE) of rear side passivated solar cells. For this experiment we used p-type FZ, 0.5 Ωcm, with a symmetrical pyramid texture resulting in 20 x 20 mm² cells.

The parasitic emitters of these solar cells were removed using the rear etching method with front side masking. Using photolithography, the front side metallization was performed, and the rear sides were dielectrically passivated with Al_2O_3. After the evaporation of a thin (2 µm) Al-layer, the rear sides were contacted by laser fired contacts and finally sintered.

As expected, the cell results show that there is a significant increase in j_{sc} of 0.5 mA/cm² between the three different rear surface morphologies. The increased rounding of the rear side random pyramid texture leads to higher IQE values in the long wavelength range between 900 and 1200 nm. IQE and reflectance of solar cells with three different rear surface morphologies are shown in Figure 11.

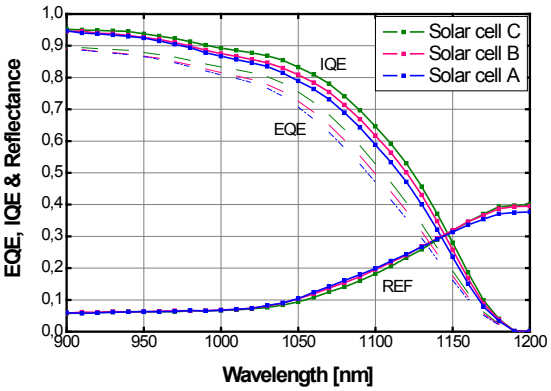

Figure 11: Measurements of EQE, IQE and reflectance of rear side passivated solar cells. The green line corresponds to a solar cell with increased pyramid rounding. The IQE of this solar cell is relatively increased by 5% in the long wavelength-range (900 nm<λ<1200 nm) due to the adapted rear-surface morphology and therefore better rear surface passivation.

Solar cell A displays the weakest rear-side texture rounding. In contrast, with solar cell C, the rear side texture was the most strongly rounded.

Although the same reflectance values were measured with the three solar cells at λ=1000 nm, the IQE values do differ significantly at this wavelength by 2.6%$_{abs}$. This can be explained by improved rear side passivation through the adapted rear side morphology. This increase of IQE values for longer wavelengths confirms the results of the lifetime studies.

The generally relatively low reflectance values on the rear side of the solar cell visible at longer wavelengths are attributable to the non-adapted dielectric layer on the rear side. Although the photolithography-based process is not yet completely adapted to alkaline textured solar cells, on the basis of the changed rear side with Al_2O_3 as passivation layer we achieved a gain in j_{sc} of 0.5 mA/cm². With a single anti-reflectance layer the mean value of j_{sc} of the improved rear side amounts to 39.1 mA/cm².

6 SUMMARY AND OUTLOOK

In this work a new procedure for the rear side etching of silicon solar cells including a masking step was presented. Therewith, three relevant approaches for solar cell processing, in particular for rear side passivated solar cells can be merged: the parasitic emitter etching, the increase of the rear side reflectance and the change of the surface morphology for better surface passivation.

First of all several acidic etch solution and their kinetics and influences on the surface morphology have been studied. Thereby, specific etch solutions show a higher etch rate on the pyramid peak than in the pyramid valley. This fact leads to a rounding of the pyramid texture with minimized material loss which is indispensable for thin silicon solar cells. The lifetime experiments have shown that a slight rounding of the rear side texture using adapted etching solutions significantly reduces the surface recombination velocity of passivated samples. S_{pass} values down to 3 cm/s for thin Al_2O_3 passivation layers were achieved.

The rear side etching procedure with masking was successfully transferred to large-size screen printed solar

cells with homogeneous emitter and full Al-BSF, whereby mean efficiencies of 18.6% and high values of shunt resistance underline the transferability of the novel procedure into industrial-like processes. The photolithography-based cell process with dielectrically passivated rear side and adapted rear surface morphology shows a gain in j_{sc} of 0.5 mA/cm².

We assume that further investigations with respect to screen-printed solar cells with selective emitter structures and rear side passivation will display more potential of this novel rear side etching procedure with masking, particularly for thin wafers in the near future.

7 ACKNOWLEDGEMENTS

The authors would like to thank N. Ximello, S. Joos, T. Lauermann, T. Lüder, J. Ebser, S. Gloger, A. Zuschlag, S. Öner, B. Terheiden, and G. Micard for their support. The financial support from the BMU project 0325079 is also gratefully acknowledged in particular for processing and characterization equipment. The content of the publication is the responsibility of the authors.

8 REFERENCES

[1] A. Aberle, *Crystalline Silicon Solar Cells*, UNSW, 1999

[2] A. Dastgheib-Shirazi et al*., Investigations of High Refractive Silicon Nitride Layers for Etched Back Emitters: Enhanced Surface Passivation for Selective Emitter Concept* , Proc. 24th EUPVSEC, 2009, Hamburg, Germany

[3] S. Dauwe, *Low-temperature rear surface passivation of crystalline silicon solar cells*, PhD thesis, University of Hannover, 2003

[4] B. Fischer, *Loss Analysis of Crystalline Silicon Solar Cells using Photoconductance ans Quantum Efficiency Measurements*, PhD Thesis, University of Konstanz, 2003

[5] S. W. Glunz et al., Comparison of Different Dielectric Passivation Layers for Application in Industrially Feasible High-Efficiency Crystalline Silicon Solar Cells, 20th EU PVSEC, 2005, Barcelona, Spain

[6] M. A. Green, *Silicon Solar Cells*, UNSW, 1995

[7] H. Haverkamp et al., Minimizing the Electrical Losses on the Front Side: Development of a Selective Emitter Process from a Single Diffusion, 33rd IEEE, 2008, San Diego, USA

[8] J. Junge et al., *Evaluating the efficiency limits of low cost mc Si materials using advanced solar cell processes*, Proc. 25th EU PVSEC, 2010, Valencia, Spain

[9] D. Kray, S. Glunz, *Investigations of Laser-fired Rear-side Recombination Properties Using an Analytical Model*, Prog. Photovolt: Res. Appl. 2006; 14: 195-201

[10] D. Kray, *Hocheffiziente Solarzellenstrukturen für kristallines Silicium-Material industrieller Qualität*, PhD Thesis, University of Konstanz, 2004

[11] B. Lenkeit, *Elektronische und strukturelle Eigenschaften von Plasma-Siliziumnitrid zur Oberflächenpassivierung von siebgedruckten, bifazialen Silizium-Solarzellen,* PhD thesis, University of Hannover, 2002

[12] T. Lüder et al*., Annealing behavior of Al_2O_3 thin films grown on crystalline silicon by atomic layer deposition, 25th EU PVSEC, 2010, Valencia, Spain*

[13] K. R. McIntosh et al., *Recombination at textured silicon surfaces passivated with silicon dioxide*, Journal of applied physics 105, 2009

[14] H. Plagwitz, *Surface passivation of crystalline silicon solar cells by amorphous silicon films*, PhD thesis, University of Hannover, 2007

[15] W. Kern, D. Puotinen, *Cleaning Solutions Based on Hydrogen Peroxide for Use in Silicon Semiconductor Technology*, RCA Review 187, 1970

[16] H. Robbins, B. Schwartz, *Chemical Etching of Silicon*, J. Electrochem. Soc. 1959, 106 (6), 505-508

[17] H. Robbins, B. Schwartz, *Chemical Etching of Silicon*, J. Electrochem. Soc., 1960, 107 (2), 108-111

[18] H. Robbins, B. Schwartz, *Chemical Etching of Silicon*, J. Electrochem. Soc., 1961, 108 (4), 365-372